electronics

MDPI

Article

A Novel Electrolytic-Free Quasi-Z-Source Ćuk LED Driver for Automotive Application

Lei Wang [1] and Wei Hu [2,*]

[1] Department of Physics and Electronic Engineering, Hanshan Normal University, Chaozhou 521041, China
[2] Experimental Center, Guangzhou University, Guangzhou 510640, China
* Correspondence: pehuwei@gzhu.edu.cn

Abstract: This paper proposes a novel electrolytic-free quasi-Z-Source Ćuk LED driver for automotive applications. Compared to the traditional Ćuk converter, the first merit of the novel converter is higher gain, which makes it apt to switch between multiple applications. Secondly, the proposed converter combines the inherent characteristics of LED load to operate in a wide range in Continuous Conduction Mode (CCM), so the inductors can assist in energy storage, and only small capacitance is required. Thirdly, inductors can be integrated and use only one core, and capacitors are electrolytic-free, which will benefit integration and long life. All merits are important to automotive application. Detailed analysis and design steps are presented. Then, with the help of the simulation software Saber, several key parts of the converter are simulated. Finally, a prototype controlled by the micro control unit stm32f103c8t6 is built, and the feasibility is verified by the experiment results.

Keywords: energy storage; renewable energy; Ćuk converter; quasi-Z-source; electrolytic-free; LED driver; automotive

Citation: Wang, L.; Hu, W. A Novel Electrolytic-Free Quasi-Z-Source Ćuk LED Driver for Automotive Application. *Electronics* **2023**, *12*, 997. https://doi.org/10.3390/electronics12040997

Academic Editors: Kent Bertilsson and Emad Samadaei

Received: 11 January 2023
Revised: 2 February 2023
Accepted: 7 February 2023
Published: 16 February 2023

1. Introduction

LEDs are increasingly preferred in automotive lighting applications for their long lifetime, mechanical robustness, and energy saving [1,2]. Batteries (12/24 V) are commonly used as the input of LED drivers in automotive applications, and different battery voltage systems are available sometimes. Therefore, LED drivers capable of operating in a wide input range are needed [3–5]. In addition, different automotive applications, such as headlights, brake lights, and turn signals, require different levels of lighting brightness, so different numbers of LEDs in series are required. Moreover, the same application may require a different number of LEDs in series (such as headlamps for high beam and low beam).

Switched-mode dc–dc converters with both step-up and step-down capability can address the above challenges. A four-switch buck–boost converter [3] is presented, whose structure can be exchanged between the buck, boost, and buck–boost to provide a desired voltage gain, but the converter efficiency drops in the buck–boost operation due to the cascaded structure. Ćuk-converter-based automotive LED drivers have also been reported [6–8]. The Ćuk converter of [6] has reduced efficiency due to hard-switching at a 500 kHz switching frequency. High-frequency Ćuk converters that achieve zero-voltage switching are presented in [7,8], but they have two or more active switches to drive, with higher complexity and more components. The latest literature is mostly based on resonant converters [4,5,9–13]. These solutions have higher efficiency and a compact size, but similar to [7,8], they usually have more switches to drive and complex structure, and variable-frequency control usually necessitates the use of large EMI filters.

Life incompatibility between electrolytic capacitors and other components of LED drivers has gradually become one of the main concerns in recent years. There are two main solutions to this problem: through new topology or control schemes [14–16]. The authors

of [17] used an inductor to assist energy storage, but the inductance is quite large because the inductor works at a low frequency.

Many new topologies have been proposed based on a quasi-Z-source network to achieve high-voltage gain [18–21]. Combining a quasi-Z-source network with the Ćuk converter, and integrating the three inductors, a novel high-gain quasi-Z-source Ćuk converter is proposed in this paper. It is suitable for a wide range of input and output, and requires small space. Because of the combination of characteristics with LED load, the converter works in CCM in a wide range, with small capacitance and long life.

This paper is organized as follows. Section 2 gives the circuit configuration and operating principle. Parameter design and control strategy are briefly described in Section 3. Then, in Section 4, the experimental results of a prototype are presented. Finally, the conclusions of this work are detailed in Section 5.

2. Circuit Configuration and Operating Principle

2.1. Circuit Configuration

The topology of the proposed quasi-Z-source Ćuk converter is shown in Figure 1 below, where L_{z1}, L_1, L_2 represent the three windings of the mutual inductors integrated on a magnetic core with the same number of turns. Compared with the traditional Ćuk converter, an inductor is replaced by the quasi-Z-source network, which is composed of L_1, L_{z1}, capacitors C_{z1}, C_{z2}, and diode D_{z1} surrounded by the sector dotted line. D_{z2} is added to suppress the low-frequency oscillation between L_1, L_{z1}, C_{z1}, C_{z2} and input V_{in} under light load. The signs and arrows in Figure 1 indicate the positive direction of capacitor voltage and inductor current, respectively.

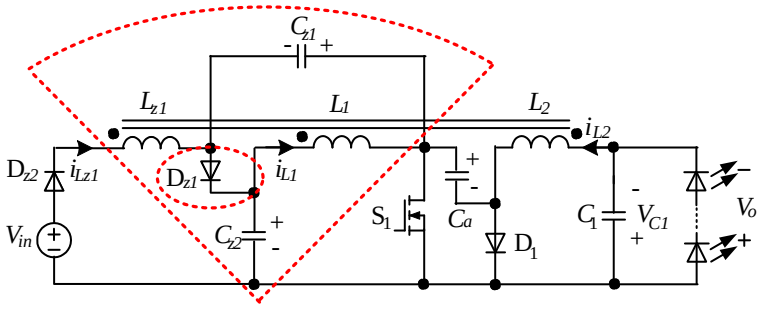

Figure 1. Proposed quasi-Z-source Ćuk LED driver.

Figure 2 shows the equivalent circuit of the quasi-Z source Ćuk Converter in four work modes in steady state. The steady-state analysis of the integrated inductor in CCM can be firstly carried out as three independent inductors, as the inductor voltage and current change in the same direction, and the coupling of inductors only causes an increase in the equivalent inductance.

The proposed converter contains three work modes as in Figure 2a–c in CCM, while it contains one more mode in Discontinuous Conduction Mode (DCM), which can be Figure 2d or Figure 2e according to the load. The arrows in Figure 2 indicate the actual direction of the loop current, and the positive and negative signs also indicate the actual direction of the element voltage. The work details are as follows:

Mode 1[t_0–t_1]: The switch S_1 is turned on at t_0, and D_{z1} is reverse-biased for $V_{cz2} > V_{cz1}$. D_1 is also off by withstanding V_{ca}. There are three current loops in this mode, and all the inductors are charged, while all the capacitors are discharging. The input voltage V_{in} and C_{z1} are connected in series to charge L_{z1}; C_{z2} charges L_1, and C_a supplies power to L_2 and the load.

Mode 2[t_1–t_2]: Mode 2 begins when S_1 is turned off. It should be noted that except C_a, all the other inductors/capacitors interchange between storing and releasing energy in this mode. The operation of the converter can be divided into three parts. V_{in} and L_{z1} are

connected in series to charge C_{z2}, L_1 charges C_{z1}, and C_a together with L_2 supplies power to C_{z1}, C_{z2}, and the load.

Mode 3[t_2–t_3]: C_a also changes to be charged in this mode, and D_1 is turned on. Therefore, all the inductors are discharging, while all the capacitors are charged. Part of i_{L1} and i_{Lz1} are in series with V_{in} to charge C_a, and the remaining current of L_1 and L_{z1} is utilized to charge C_{z1} and C_{z2} separately. At the same time, L_2 freewheels through D_1 and charges the load.

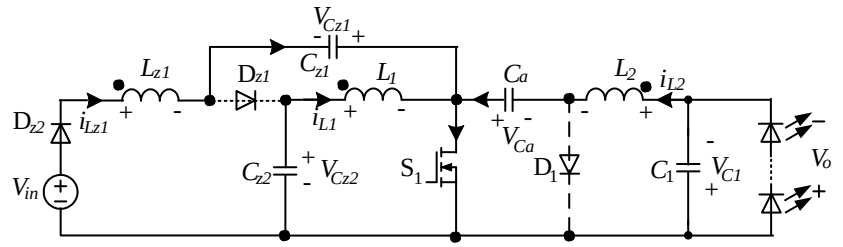

(a) Mode 1, S_1 is on, and all inductors are charged by the capacitors.

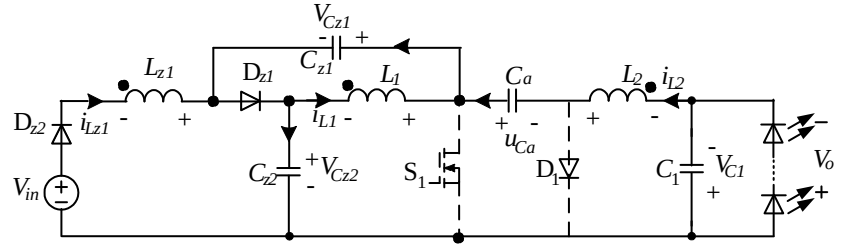

(b) Mode 2, S_1 is off, and all capacitors but Ca are charged by the inductors.

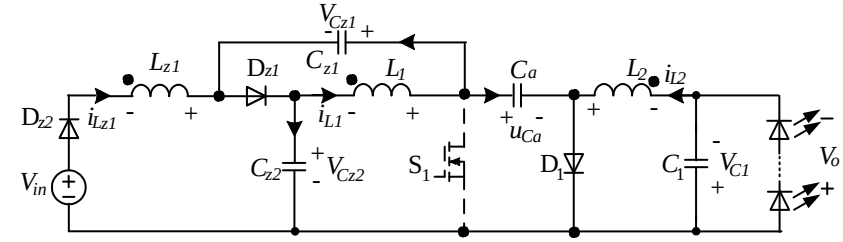

(c) Mode 3, S_1 is off, all capacitors are charged by the inductors.

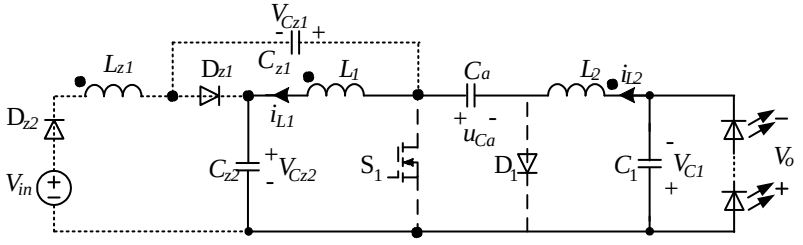

(d) Mode4-1, light discontinuous mode.

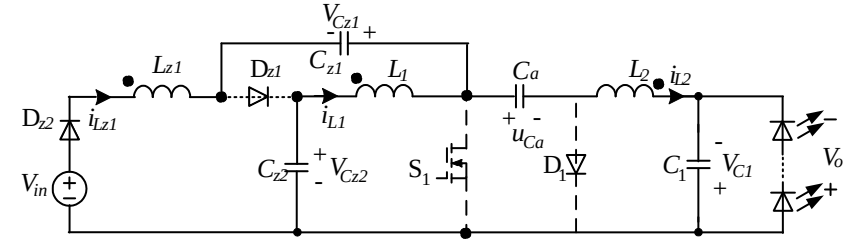

(e) Mode4-2, deep discontinuous mode.

Figure 2. Equivalent circuit of the proposed driver with four possible work modes.

Figure 3 presents the current and voltage waveforms on the integrated three inductors, and the current waveform of C_a, where t_s is the switching cycle, and d_1, d_2, and d_3 are the duty ratios corresponding to the duration of modes 1, 2, and 3, respectively. It is easy to understand that the voltage waveforms on the integrated three inductors are the same with the same number of turns, but the current waveforms of i_{L1} and i_{Lz1} are different from i_{L2}.

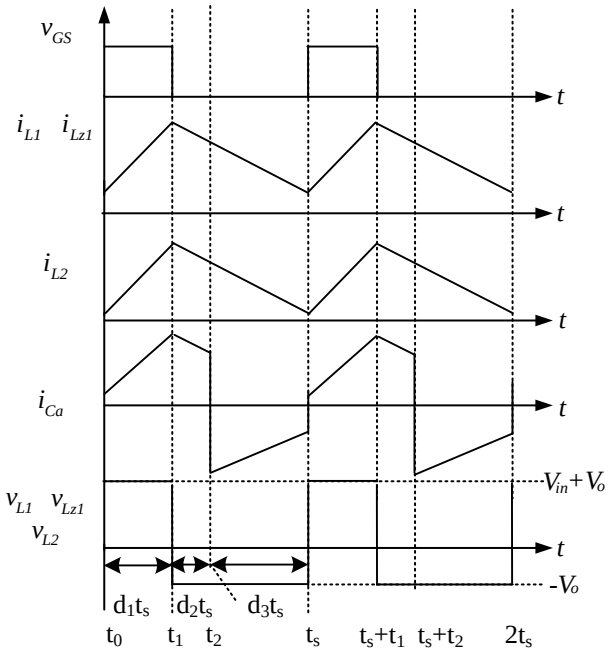

Figure 3. Theoretical waveforms of the proposed converter in CCM.

If the load is light enough, the converter will enter into DCM, and the converter has a fourth mode in a switching cycle as in Figure 2d,e, where the switch and diodes are always off.

Mode 4-1[t_3–t_s]: i_{Lz1} cannot be reversed due to D_{z2} in light discontinuous mode, so it remains zero. The slew rate of i_{Lz1} is zero, and the voltage on L_{z1} is also zero, resulting in zero voltage on other windings of the mutual inductor at the same time. There is only one current loop: C_a charges C_1 and C_{z2}, and i_{L1} and i_{L2} basically stay constant at this stage.

Mode 4-2[t_3–t_s]: Since the output current is very small and the output voltage is also higher in deep discontinuous mode, i_{L2} drops faster than i_{L1} and i_{Lz1} to negative at the end of mode 3, while i_{L1} and i_{Lz1} remain positive. The only thing that happens is that C_{z1}, $C_{z2,}$ and C_1 charge C_a with a constant current in this interval.

The theoretical waveforms of the proposed converter in DCM are presented in Figure 4 below. If the converter is just at the boundary of CCM and DCM, that is in Boundary Current Mode (BCM), i_{Lz1} is zero at the end of the cycle. Note that there is no time that all winding currents are zero in this DCM, but the total magnetic flux of the core is zero during mode 4. Although the mutual inductor is designed to have the same name end when the voltage is applied, the reverse current always appears in DCM, which may actually reduce the equivalent inductance.

The major feature is that the charging and discharging of the capacitors are always in series with the inductors, resulting in a smooth variation of the capacitor voltage. Therefore, the inductances and capacitances can be relatively small, which is good for integration and heat dissipation.

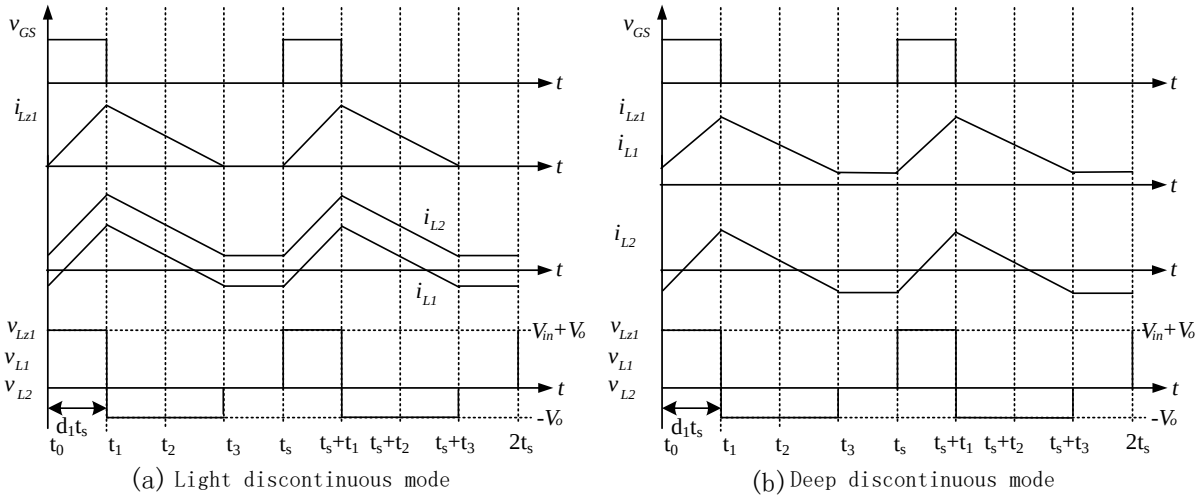

Figure 4. Theoretical waveforms of the proposed converter in DCM.

2.2. General Analysis

In the following analysis, the switch and diodes are assumed to be ideal. The voltage on L_{z1}, L_1, L_2 in CCM are given by Equations (1) and (2) below according to mode 1–3. Note that the equations of inductor voltage for mode 2 and 3 are the same:

$$\begin{cases} V_{in} + V_{cz1} = V_{Lz1} \\ V_{cz2} = V_{L1} \\ V_{ca} = V_{L2} + V_o \end{cases} \tag{1}$$

$$\begin{cases} V_{in} + V_{Lz1} = V_{cz2} \\ V_{L1} = V_{cz1} \\ V_{cz2} + V_{L1} = V_{ca} \\ V_{L2} = V_o \end{cases} \tag{2}$$

Since the voltages on L_{z1}, L_1, L_2 are the same, the relationship between the capacitor voltages can be inferred from Equations (1) and (2):

$$\begin{cases} V_{cz2} = V_{in} + V_{cz1} \\ V_{ca} = V_{cz1} + V_{cz2} \end{cases} \tag{3}$$

Then the following relationship can be obtained from the volt-second balance of L_{z1}, L_1, and L_2:

$$\begin{matrix} L_{z1} \\ L_1 \\ L_2 \end{matrix} \begin{cases} d_1(V_{in} + V_{cz1}) = (d_2 + d_3)(V_{cz2} - V_{in}) \\ d_1 V_{cz2} = (d_2 + d_3) V_{cz1} \\ d_1(V_{ca} - V_o) = (d_2 + d_3) V_o \end{cases} \tag{4}$$

Substituting Equation (3) into Equation (4), from the volt-second balance relationship of L_1 and L_2 we can get $V_{cz1} = V_o$. Then, plugging it into the volt-second balance equation of L_{z1} in Equation (4), and eliminating V_{cz1} and V_{cz2}, yields the important relationship among input, output voltage, and duty ratio:

$$d_1(V_{in} + V_o) = (d_2 + d_3)\left(\frac{d_2 + d_3}{d_1} V_o - V_{in}\right) \tag{5}$$

There is no mode 4 in CCM, so the relationship of duties becomes: $d_2 + d_3 = 1 - d_1$. Substituting this into Equation (5), the expression for the output voltage in CCM is given by:

$$V_o = V_{in} \frac{d_1}{(1 - 2d_1)} \tag{6}$$

This relationship looks similar to the basic converters, where the output voltage is not directly related to the output current in CCM. Further analysis needs to introduce the current equation corresponding to the capacitor's charge balance:

$$\begin{matrix} C_{z1} \\ C_{z2} \\ C_a \end{matrix} \begin{cases} d_1 I_{Lz1} = d_2(I_{L1} + I_{L2}) + d_3 \alpha I_{L1} \\ d_1 I_{L1} = d_2(I_{Lz1} + I_{L2}) + d_3 \beta I_{Lz1} \\ (d_1 + d_2) I_{L2} = d_3(1 - \alpha) I_{L1} \end{cases} \tag{7}$$

where α and β are the scale factors when i_{L1} and i_{lz1} are divided into two parts in mode 3, respectively. Since L_1 and L_{z1} charge C_a in series in mode 3, the current is equal, i.e.,

$$(1 - \alpha) I_{L1} = (1 - \beta) I_{Lz1} \tag{8}$$

Regarding the circuit containing D_{z1} enclosed by the dashed ellipse in Figure 1 as a node, Kirchhoff's current law can be applied. Because of charge balance, the average current of C_{z1} and C_{z2} in a whole cycle is zero, so a new current relationship is achieved:

$$I_{L1} = I_{Lz1} \tag{9}$$

Synthesizing Equations (8) and (9), we know α = β. After substituting it back into Equation (7), we find that C_{z1} and C_{z2} are charged and discharged in the same way, and their charge balance equations are the same. According to mode 3, C_{z1} and C_{z2} are both charged by the current αI_{L1}, and C_a is charged by the current $(1 - \alpha) I_{L1}$. The three capacitors form a voltage loop, so the voltage increment of these capacitors should be equal, that is:

$$\Delta V_{ca} = (1 - \alpha) I_{L1} / C_a = \Delta V_{cz1} + \Delta V_{cz2} = \alpha I_{L1} / C_{z1} + \alpha I_{L1} / C_{z2} \tag{10}$$

Eliminate I_{L1} from Equation (10) and simplify the expression to obtain:

$$\alpha = 1 / (1 + C_a / C_{z1} + C_a / C_{z2}) \tag{11}$$

Thus, α is determined by the capacitance ratio. From Figure 2d or Figure 2e in mode 4, we know that:

$$V_{ca} = V_o + V_{cz2} \tag{12}$$

Comparing Equations (12) and (3), we can infer that $V_{cz1} = V_o$, and $V_{ca} = V_{in} + 2V_o$.

The output voltage gain of the traditional Ćuk converter is $d_1/(1 - d_1)$ in CCM. Figure 5 below shows the gain comparison between the traditional and the proposed Ćuk converter, whose gain is based on Equation (6). It can be seen that the output voltage of the quasi-Z-source converter is much larger than that of the traditional Ćuk converter in CCM.

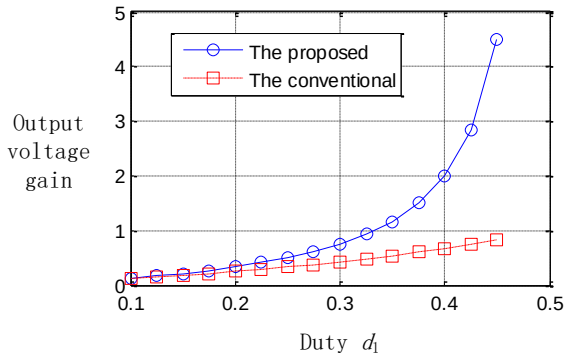

Figure 5. Gain comparison between the traditional and the proposed Ćuk converter in CCM.

3. Parameter Design and Control Strategy

3.1. Boundary Analysis

The inductor can help to store energy only in CCM mode. Furthermore, the reverse flow of current occurs in DCM lead to lower efficiency. Therefore, the converter should be designed to operate in CCM, and the boundary current from CCM to the light DCM with a decrease in load current should be estimated, since i_{Lz1} is zero at the end of the cycle in BCM, and the waveform of i_{Lz1} in one cycle is triangular. According to the triangle area formula, the peak value is twice the average value. Therefore, it can be obtained from the analysis of mode 1 based on Faraday's law of electromagnetic induction:

$$(V_{in} + V_{cz1})d_1 t_s / L_{z1} = \Delta i_{Lz1} = 2I_{Lz1} \tag{13}$$

It is necessary to model the LED load to calculate the boundary load current. A single LED is modeled as a series connection of an ideal diode, a voltage source, and a resistor, similar as in [12]. The model circuit and its parameters used in the following analysis are shown in the Figure 6 below. The linearized model can be obtained by making a tangent at the rated current on the nonlinear voltage and current curve of power LED Luxeon LXM3-PW81 [22] used in the experiment, and the corresponding parameters can be achieved. Note that temperature factor is ignored here.

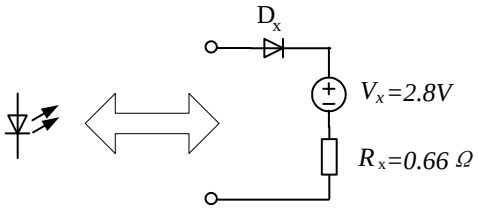

Figure 6. Single LED model parameter.

According to this LED model, the output voltage can be obtained from I_o:

$$V_o = N_{led} * V_x + R_x * N_{led} * I_o \tag{14}$$

where N_{led} represents the number of LEDs in the load.

Given V_{in}, L_{z1}, and LED load, I_o is initialized to be zero, V_o can be achieved through Equation (13). Three steps are taken to obtain the BCM load current, which is utilized to design the integrated inductor in the next subsection.

1. d_1 can be obtained from Equation (6), and the boundary current I_{Lz1} can be inferred from Equation (13).
2. From the balance of input and output power, we know that:

$$V_{in} I_{Lz1} = V_o I_o \tag{15}$$

3. Then Io can be obtained.
4. A new Vo is calculated through Equation (14). The iteration stops when the error of Vo obtained by the two adjacent iterations is small enough, or we return to step 1.

When the error is set to 0.0001, less than 5 iterations are needed for a certain LED load.

3.2. Integrated Inductor Design

The design of the integrated inductor is decided by the CCM range of the load. The load current curve of BCM under different input voltages and different self-inductance of L_{z1} is shown in Figure 7 based on the numerical iteration algorithm in the previous subsection. It can be seen that the boundary load current increases significantly with the increase in input voltage, and slightly increases with the decrease in the LED load.

A self-inductance of 150 μH is selected to guarantee the converter to work in CCM in a wide range.

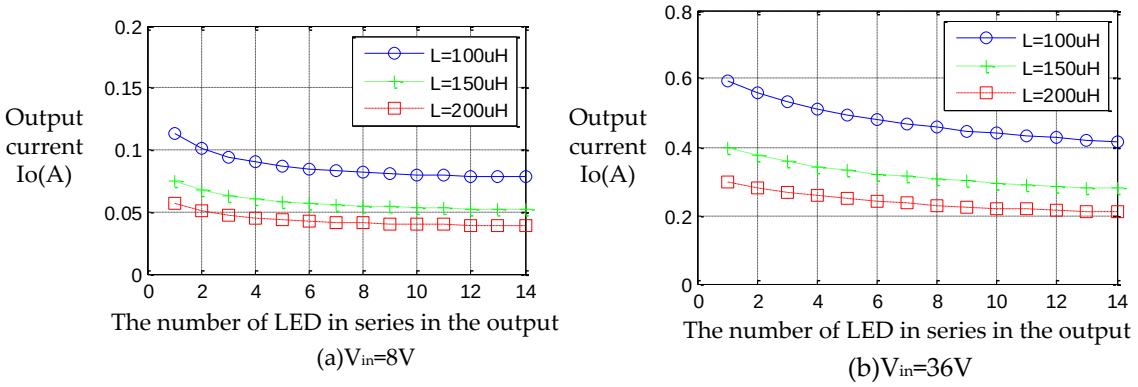

Figure 7. Output boundary current in different input voltages with different self-inductance.

3.3. Circuit Control

Figure 8 shows the control block diagram of the proposed converter. To avoid excessive current during startup, soft startup is set in the program. At the beginning of startup, a slightly large duty is set for the converter for open-loop operation. The incremental current closed-loop PI duty cycle control is activated when the output current reaches within a certain range. Note that the output voltage of the proposed Ćuk converter is negative, so the potential of the sampling current on R_s is negative. A level-raising circuit is added to make it positive, and then the subsequent signal conditioning circuit and PI block are used to perform closed-loop control.

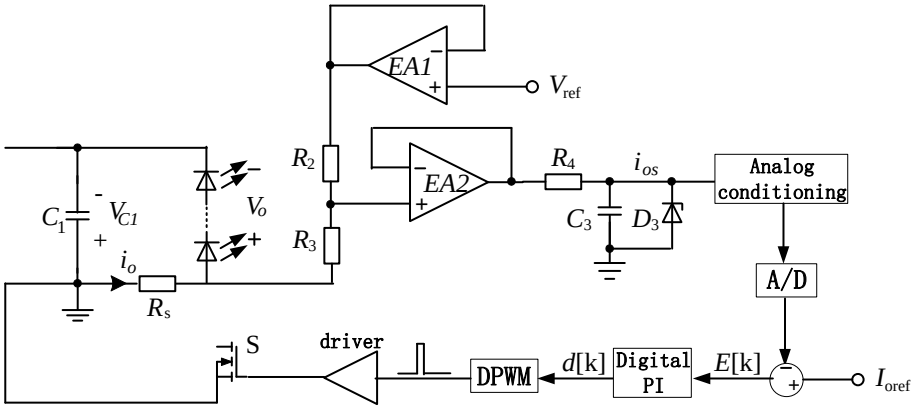

Figure 8. Control block diagram of the proposed LED driver.

4. Simulation and Experimental Verification

The key of this converter simulation is the modeling of the multi-winding coupling inductor, which has been discussed in many studies recently [23,24]. Saber is a simulation software that can help. For the simulation model of mutual inductors, the coupling coefficient between windings should be defined in pairs, so three inductors and three coupling coefficients should be defined for three winding coupled inductors, as shown in Figure 9 below. In order to obtain a more accurate coupling coefficient, the windings of the fabricated coupling inductor are connected in series to measure mutual inductance in pairs. After obtaining the self-inductance of each winding, the simulation model is established.

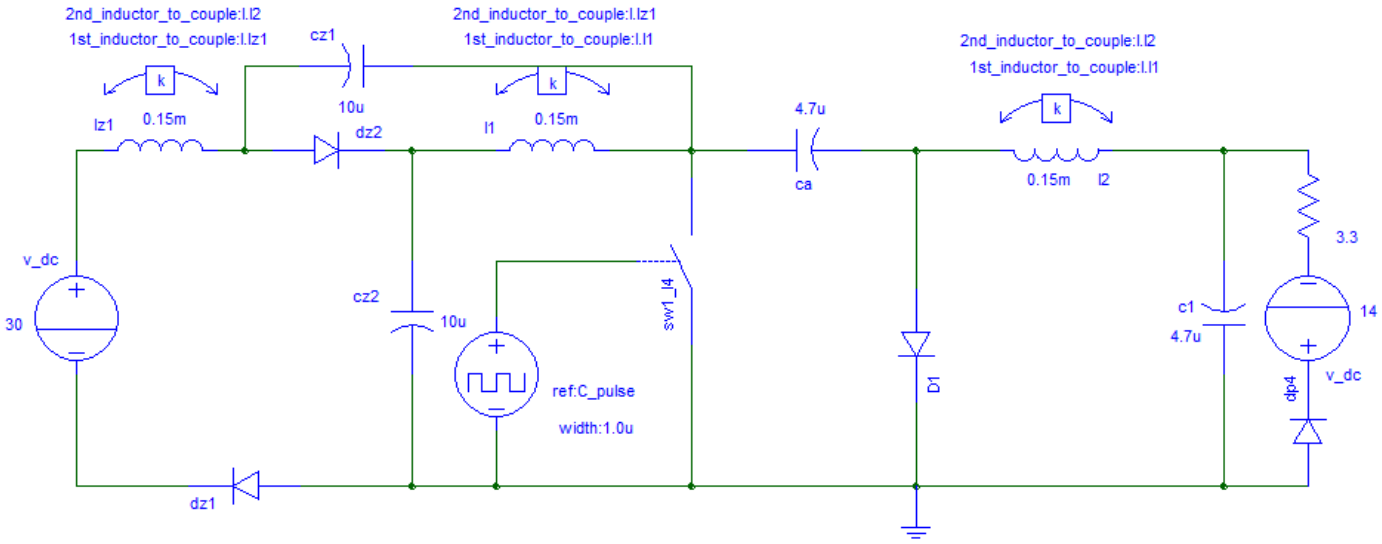

Figure 9. Open-loop simulation circuit.

The simulation waveform in Figure 10 presents the operation waveforms of two DCM modes under different load current. In Figure 10a, iLz1 remains zero in the fourth mode, while iL1 is negative and iL2 is positive. In Figure 10b, both iLz1 and iL1 remain positive, while iL2 is negative for a period of time. The verification of the operation waveform of DCM mode provides the basis for the design of the integrated inductor, and also validates the theoretical analysis in the previous section.

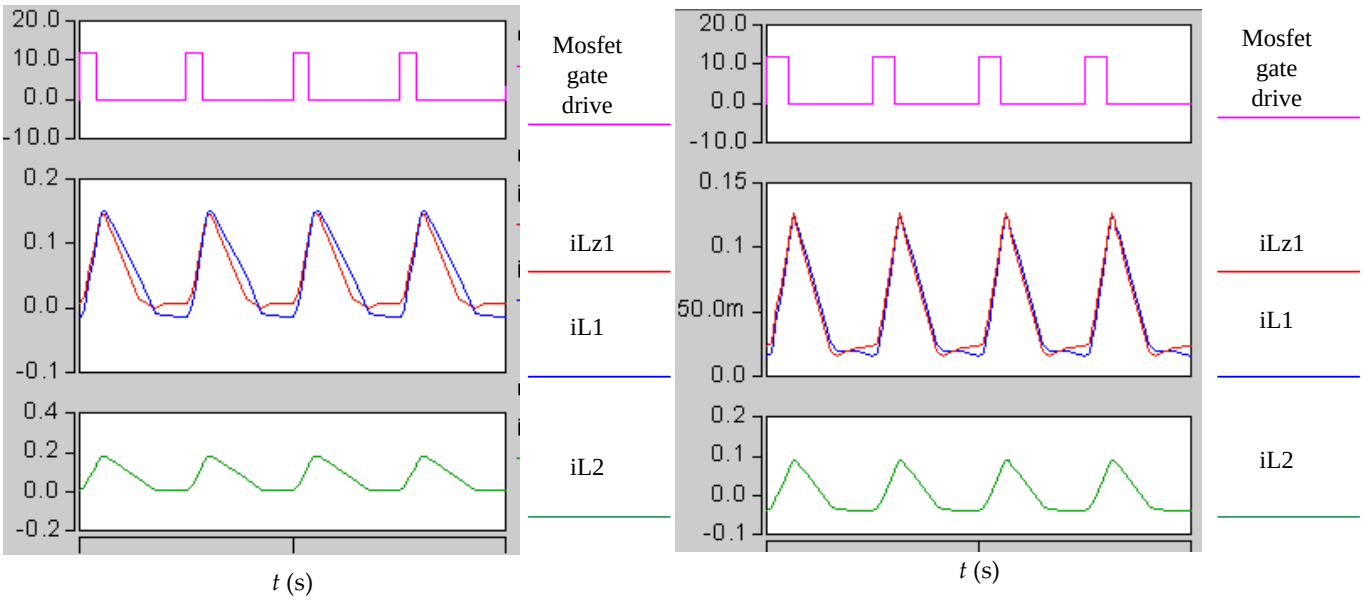

Figure 10. Simulation waveforms of the DCM operation. (**a**) Light discontinuous operation waveform; (**b**) deep discontinuous operation waveform.

To verify the validity of the proposed LED driver, a prototype, shown in Figure 11, has been built and tested. The key components used in the prototype are listed in Table 1, and the control is realized by a micro control unit (stm32f103c8t6). The load consists of one LED string, according to the number of LEDs, and the output voltage ranges from 6 V to 36 V.

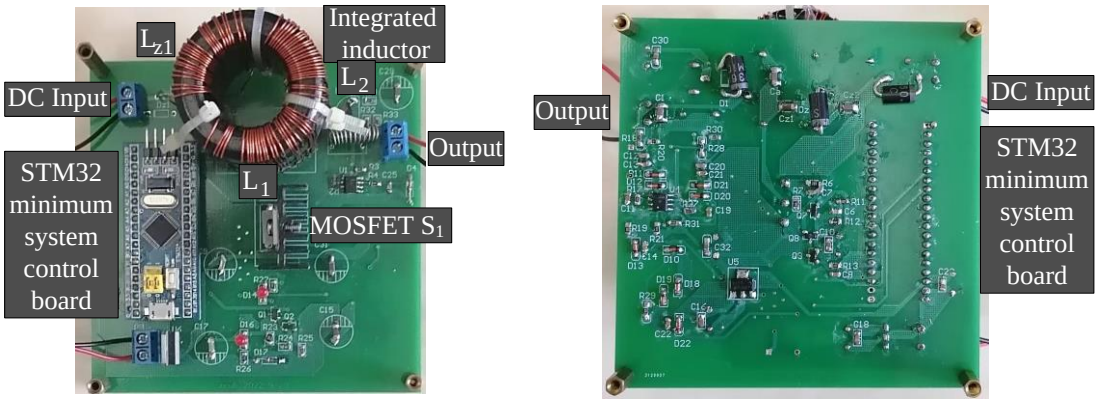

(**a**) (**b**)

Figure 11. Photograph of the prototype. (**a**) Front view; (**b**) back view.

Table 1. Key parameters of the protype.

Parameter	Value	Parameter	Value
Input voltage V_{in}	8 V–36 V	Capacitor C_{z1}, C_{z2}	10 µF
Number of LED in series	2–12	Capacitor C_a, C_1	4.7 µF
Rated load current	0.5 A	Switching frequency f_s	100 KHz
Self-inductance of L_1, L_{z1}, L_2	150 µH	N-MOSFET S_1	FQPF28N15/16.7 A, 150 V
D_1, D_{z1}, D_{z2}	SR5150/5 A, 150 V		

Figure 12 shows the startup waveform of I_o, V_o, and V_{ca} under a load of 2 LEDs and 12 LEDs in series with rated 0.5 A current, respectively. Before startup, V_{ca} is equal to V_{in}; when S_1 obtains the effective drive, V_{ca} and V_o change immediately. Note that the output voltage is negative. It can be seen from the experimental waveform that the dynamic characteristics of the converter are relatively fast under different loads.

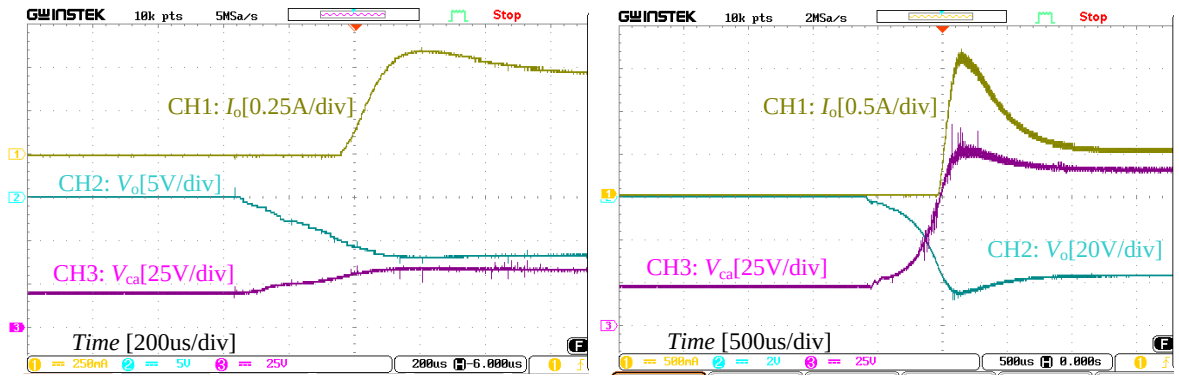

t (s) t (s)

(**a**) (**b**)

Figure 12. Startup waveforms of I_o, V_o, and V_{ca} under different loads. (**a**) Output load with 2 LEDs in series; (**b**) output load with 12 LEDs in series.

Figure 13 displays the steady-state waveform of I_o, V_o, and V_{ca} under the load of 2 LEDs and 12 LEDs with rated 0.5 A current, respectively. It is indicated that the output is quite stable, and the output ripple current is less than 10% under the rated load.

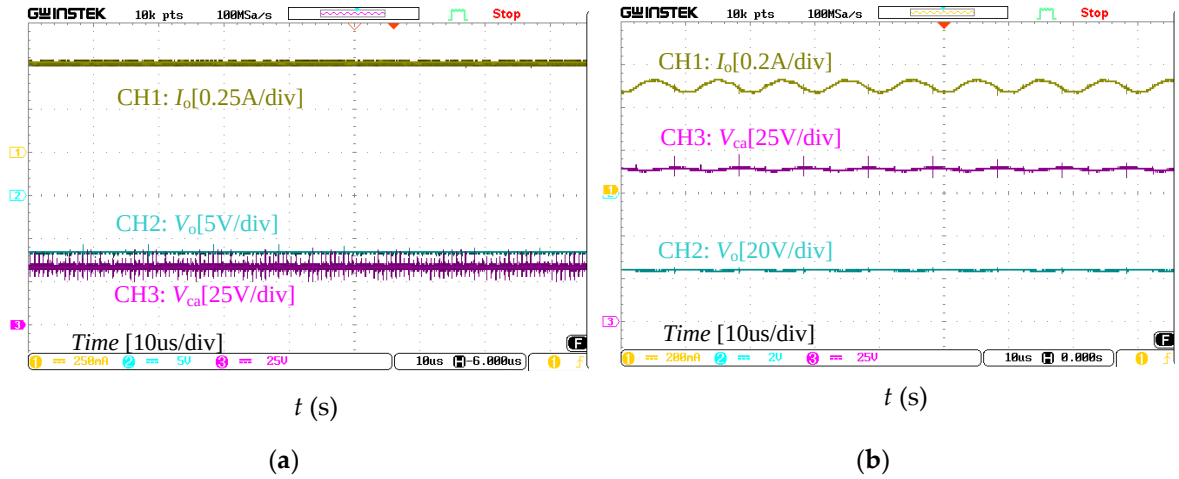

Figure 13. Steady-state waveforms of I_o, V_o, and V_{ca} under different loads. (**a**) Output load with 2 LEDs in series; (**b**) output load with 12 LEDs in series.

Figure 14 shows the efficiency of the converter when the input voltage range is 8–36 V, where the corresponding number of load LEDs in series N_{led} is 2,6,10,12, and the rated output current is 0.5 A. It can be seen that the system efficiency increases gradually with the increase in input voltage and load. As the input voltage increases, the input current decreases, and the switch turn-off voltage rises. However, the decrease in the input current seems to have a greater impact on the efficiency.

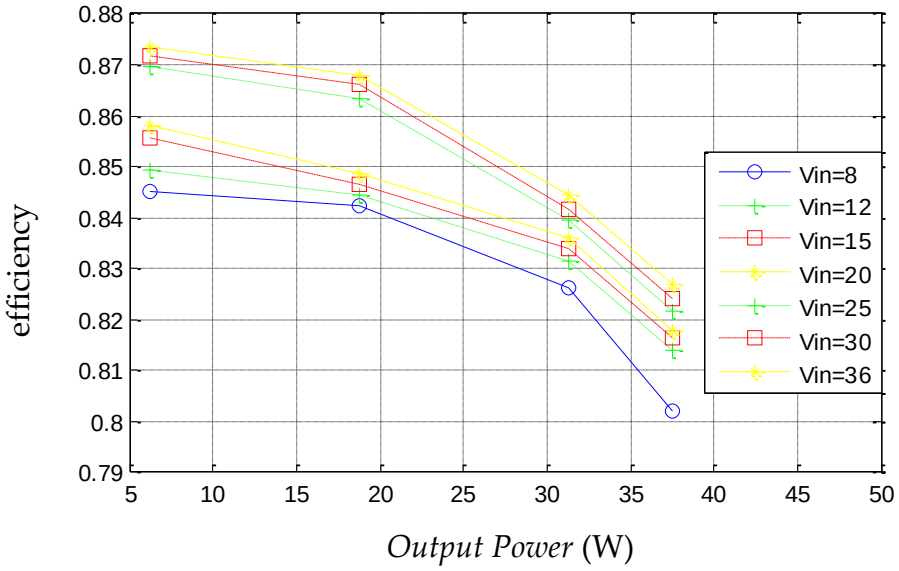

Figure 14. Measured efficiency with input voltage ranging from 8 to 36 V under different LED loads.

5. Conclusions

In this paper, a novel quasi-Z-source Ćuk converter topology is proposed, and its work mode is analyzed in detail. Compared with the traditional Ćuk converter, its output voltage gain is greatly improved, which makes it more apt for wide input and load changes. Furthermore, the proposed converter combines the inherent characteristics of LED load to operate in a wide range in CCM, so the inductor can assist in energy storage, and electrolytic-free is available when small capacitance is required. In addition, inductors can be integrated and use only one core. Therefore, the converter requires less space. Finally, the feasibility of the proposed new topology is verified by experiments.

Author Contributions: Formal analysis, L.W.; Project administration, W.H.; Validation, W.H.; Writing—original draft, L.W.; Writing—review & editing, L.W. and W.H. All authors have read and agreed to the published version of the manuscript.

Funding: This research was funded by Hanshan Normal University, Dr. Scientific Research Fund, grant number QD20180126 and the Guangdong Basic and Applied Basic Research Foundation under grant 2021A1515010616.

Data Availability Statement: Not applicable.

Conflicts of Interest: The authors declare no conflict of interest.

References

1. Pollock, A.; Pollock, H.; Pollock, C. High efficiency LED power supply. *IEEE Trans. Emerg. Sel. Top. Power Electron.* **2015**, *3*, 617–623. [CrossRef]
2. Gacio, D.; Cardesin, J.; Corominas, E.L.; Alonso, J.M.; Dalla-Costa, M.; Calleja, A.J. Comparison among power LEDs for automotive lighting application. In Proceedings of the IEEE Industry Applications Society Annual Meeting (IAS), Edmonton, AB, Canada, 5–9 October 2008.
3. Qin, Y.; Li, S.; Hui, S.Y. Topology-transition control for wide-input-voltage-range efficiency improvement and fast current regulation in automotive LED application. *IEEE Trans. Ind. Electron.* **2017**, *64*, 5883–5893. [CrossRef]
4. Mukherjee, S.; Yousefzadeh, V.; Sepahvand, A.; Doshi, M. A two-stage automotive LED driver with multiple outputs. *IEEE Trans. Power Electron.* **2021**, *36*, 14175–14186. [CrossRef]
5. Veeramallu, S.; Narasimharaju, B.L.; Porpandiselvi, S. A non-isolated wide input series resonant converter for automotive LED lighting system. *IEEE Trans. Power Electron.* **2021**, *36*, 5686–5699. [CrossRef]
6. Corradini, L.; Spiazzi, G. A high-frequency digitally controlled LED driver for automotive applications with fast dimming capabilities. *IEEE Trans. Power Electron.* **2014**, *29*, 6648–6659. [CrossRef]
7. Sepahvand, A.; Kumar, A.; Doshi, M.; Yousefzadeh, V.; Patterson, J.; Afridi, K.K.; Maksimović, D. Automotive LED driver based on high frequency zero voltage switching integrated magnetic Ćuk converter. In Proceedings of the IEEE Energy Conversion Congress and Exposition (ECCE), Milwaukee, WI, USA, 18–22 September 2016.
8. Sepahvand, A.; Kumar, A.; Doshi, M.; Yousefzadeh, V.; Patterson, J.; Afridi, K.K.; Maksimović, D. High-frequency ZVS Ćuk converter for automotive LED driver applications using planar integrated magnetic. In Proceedings of the Applied Power Electronics Conference and Exposition (APEC), Tampa, FL, USA, 26–30 March 2017.
9. Wang, Y.; Gao, S.; Guan, Y.; Huang, J.; Xu, D.; Wang, W. A single-stage LED driver based on double LLC resonant tanks for automobile headlight with digital control. *IEEE T. Transp. Electr.* **2016**, *2*, 357–368. [CrossRef]
10. Khatua, M.; Kumar, A.; Yousefzadeh, V.; Sepahvand, A.; Doshi, M.; Maksimović, D.; Afridi, K.K. High-performance megahertz-frequency resonant dc-dc converter for automotive LED driver applications. *IEEE Trans. Power Electron.* **2020**, *35*, 10396–10412. [CrossRef]
11. Mukherjee, S.; Yousefzadeh, V.; Sepahvand, A.; Doshi, M.; Maksimović, D. High frequency wide range resonant converter operating as an automotive LED driver. *IEEE Trans. Emerg. Sel. Topics Power Electron.* **2021**, *9*, 5781–5794. [CrossRef]
12. Yang, L.; Yu, W.; Zhang, J. Variable frequency constant current control method for switched-capacitor converter based automotive LED driver. *IEEE Access* **2019**, *7*, 42094–42106. [CrossRef]
13. Molavi, N.; Farzanehfard, H. Load-independent hybrid resonant converter for automotive LED driver applications. *IEEE Trans. Power Electron.* **2022**, *37*, 8199–8206. [CrossRef]
14. Salazar-Pérez, D.; Ponce-Silva, M.; Alonso, J.M.; Aquí-Tapia, J.A.; Cortés-García, C. A novel high-power-factor electrolytic-capacitor-less LED driver based on ripple port. *IEEE Trans. Emerg. Sel. Topics Power Electron.* **2021**, *9*, 6248–6258. [CrossRef]
15. Brand, J.S.; Abdelmessih, G.Z.G.; Alonso, J.M.; Wang, Y.; Guan, Y.; Dalla Costa, M.A. Capacitance reduction in flicker-free integrated off-line LED drivers. *IEEE Trans. Ind. Electron.* **2021**, *68*, 11992–12001. [CrossRef]
16. Li, H.; Li, S.; Xiao, W. Single-phase LED driver with reduced power processing and power decoupling. *IEEE Trans. Power Electron.* **2021**, *36*, 4540–4548. [CrossRef]
17. Ye, C.; Das, P.; Sahoo, S.K. Inductive decoupling based multi-channel LED driver without electrolytic capacitors. *IET Power Electron.* **2019**, *12*, 2771–2779. [CrossRef]
18. Ding, X.; Wang, F.; Zhou, M.; Cao, Y.; Wei, Z. Soft switching high voltage gain Quasi-Z-Source DC–DC converter with switched-capacitor technique. *IEEE Trans. Ind. Electron.* **2022**, *69*, 11231–11241. [CrossRef]
19. Samadian, A.; Hosseini, S.H.; Sabahi, M. A new three-winding coupled inductor nonisolated Quasi-Z-Source high step-up DC–DC converter. *IEEE Trans. Power Electron.* **2021**, *36*, 11523–11531. [CrossRef]
20. Hong, D.; Cha, H. LED current balancing scheme using current-fed Quasi-Z-Source converter. *IEEE Trans. Power Electron.* **2021**, *36*, 14187–14194. [CrossRef]
21. Veerachary, M.; Kumar, P. Analysis and design of quasi-z-source equivalent dc–dc boost converters. *IEEE T. Ind. Appl.* **2020**, *56*, 6642–6656. [CrossRef]
22. Luxeon LXK2 White LED Datasheet, DS51. 2006. Available online: http://www.lumileds.com (accessed on 11 May 2018).

23. Kang, T.; Gandomkar, A.; Lee, J.; Suh, Y. Design of optimized coupling factor for minimum inductor current ripple in dc-dc converter using multiwinding coupled inductor. *IEEE T. Ind. Appl.* **2021**, *57*, 3978–3989. [CrossRef]
24. Zaoskoufis, K.; Tatakis, E.C. A thorough analysis for the impact of the coupling coefficient on the behavior of the coupled inductor high step-up converters. *IEEE Trans. Power Electron.* **2020**, *35*, 8287–8302. [CrossRef]